A&A 409, 263–274 (2003)
DOI: 10.1051/0004-6361:20030978

Astronomy & Astrophysics

The corona of HD 223460 (HR 9024)

P. Gondoin⋆

European Space Agency, ESTEC – Postbus 299, 2200 AG Noordwijk, The Netherlands

Received 13 December 2002 / Accepted 19 June 2003

Abstract. HD 223460 (HR 9024), a chromospherically active late−type giant with a high X-ray luminosity, was observed by the *XMM–Newton* space observatory. Series of lines of highly ionized Fe and several Lyman lines of hydrogen-like ions and triplet lines of helium-like ions are visible in the reflection grating spectra, most notably from O and Ne. Analysis results suggest a scenario where the corona of HD 223460 is dominated by large magnetic structures similar in size to interconnecting loops between solar active regions but significantly hotter. The surface area coverage of these active regions may approach up to 30%. A hypothesis is that the interaction of these structures themselves induces a flaring activity on a small scale not visible in the EPIC light curves that is responsible for heating HD 223460 plasma to coronal temperatures of $T \geq 10^7$ K. The intense X-ray activity of HD 223460 is related to its evolutionary position at the bottom of the red giant branch. It is anticipated that its rotation will spin down in the future with the effect of decreasing its helicity-related, dynamo-driven activity and suppressing large-scale magnetic structures in its corona.

Key words. stars: individual: HD 223460 – stars: activity – stars: coronae – stars: evolution – stars: late-type – X-rays: stars

1. Introduction

HD 223460 (HR 9024) is a chromospherically active late−type giant. Cowley & Bidelman (1979) indicate that the Ca II emission in this star is moderately strong while Bopp (1984) notes that the H and K emission fluxes are quite high, comparable to what is observed in FK Comae. Feldman (1982) detected HD 223460 as a radio source and initially suggested that HD 223460, which apparently exhibits no detectable velocity variation, is an FK Comae type star. Cowley & Bidelman (1979) classified HD 223460 as a G1 III star but its $B-V$ color is too large for the assigned MK type which suggests unusual reddening for the distance (Ayres et al. 1998). HD 223460 shows some Li I absorption (De Medeiros & Lebre 1992), a sign of evolutionary youth and lack of deep mixing (Wallerstein et al. 1994) consistent with its spectral type and luminosity class which indicate that the star recently became a giant. Its rotation velocity ($v \sin i = 20$ km s^{-1}; Fekel et al. 1986) is low for an FK Comae type star and Bopp (1984) suggested that the star could be seen pole-on. This moderate $v \sin i$ of 21.6 ± 1.0 km s^{-1} confirmed by Medeiros & Lebre (1992) is comparable with the photometric rotation period of 23 days measured by Strassmeier & Hall (1988) for a normal $\approx 10\ R_\odot$ giant. Another characteristic of HD 223460 includes an X-ray luminosity (Singh et al. 1996; Hünsch et al. 1998) exceptionally high for a red giant, similar to that of an FK comae type star (Gondoin 1999). I report on analysis results of X−ray spectra of HD 223460 registered during two observations performed in July 2000 and in January 2001 by the *XMM–Newton* observatory. The observations were conducted with the aim to improve our understanding of the magnetic activity on HD 223460 by investigating the origin of its high X-ray luminosity and the structure of its X-ray corona.

This paper is organized as follows. Section 2 provides the stellar parameters of HD 223460 and compares the evolution status of this star with those of nearby single field giants in light of Hipparcos parallaxes (ESA 1997). Section 3 describes the X-ray observations of HD 223460 and the data reduction procedures. Section 4 then presents the integrated flux measurements and their temporal behavior during the observations. Section 5 describes the spectral analysis of the datasets obtained with the European Photon Imaging Camera (EPIC) and the Reflection Grating Spectrometer (RGS) on board *XMM–Newton*. Finally, a physical interpretation of the analysis results is proposed in Sect. 6. In this last section, the structure of HD 223460 corona and its possible evolution is discussed within the frame of stellar activity evolution across the Hertzsprung gap.

2. HD 223460 stellar parameters

A differential *UBV* photometry study performed by Strassmeier & Hall (1988) indicates a *V* magnitude amplitude variation of 0.065 on HD 223460 presumably due to spot activities in the photosphere of the star. Since reliable measurements of the minimum *V* magnitude were not found, an upper estimate of the maximum luminosity of HD 223460 was obtained by subtracting the above *V* amplitude variation from the *V* Johnson magnitude specified in the Hipparcos catalogue. The visual extinction of the star was calculated by applying Chen et al. (1998) model with the upper distance limit

⋆ e-mail: pgondoin@rssd.esa.int

Table 1. Top: V magnitude, parallax and absolute magnitude of HD 223460. Middle: spectral type, color indices and effective temperature. Bottom: estimated stellar parameters of HD 223460.

V	par (mas)	M_V
5.86	7.41 ± 0.70	–0.03 +0.34
$B-V$	$V-I$	$T_{\rm eff}$ (K)
0.806	0.83	5110
R ($R_\odot$)	$v_{\rm eq}$ (km s^{-1})	M ($M_\odot$)
10–13	23–28	2.8–3.1

derived from the Hipparcos catalogue. The visual extinction is smaller than the magnitude variation due to rotational modulation by photospheric spots. The absolute magnitude was calculated from the V magnitude, visual extinction and Hipparcos parallax (see Table 1). The stellar luminosity was then derived using the bolometric correction vs. effective temperature data of Flower (1996).

Figure 1 shows the position of HD 223460 in the H–R diagram compared with evolutionary tracks inferred from grids of stellar models with a near solar metallicity ($Z = 0.02$) provided by Schaller et al. (1992). The models use opacities provided by Rogers & Iglesias (1991) and Kurucz (1991) and their convection parameters (i.e. mixing length ratio and overshooting parameter) have been calibrated using the red giant branch (RGB) of a wide range of clusters. The mass of HD 223460 was estimated to 2.8–3.1 $M_\odot$ from its position with respect to the theoretical evolutionary tracks. The star most likely originates from an early B type, single star as it evolves in the giant domain. Li abundance measurements (Wallerstein et al. 1994) support this scenario where the star has recently become a giant and is crossing the Hertzsprung gap prior the lithium depletion by convective dilution. At a later evolutionary stage when the star ascends the red giant branch, the inward expansion of its convective envelope would be expected to transport Li from the surface to the interior thus reducing its surface abundance.

The radius of HD 223460 was calculated from its luminosity and effective temperature. The photometric period (P = 23 days; Strassmeier & Hall 1988) and the radius of the star were then used to estimate its equatorial velocity (see Table 1). Comparison with the projected rotational velocity ($v \sin i = 21.6 \pm 1.0$ km s^{-1}; de Medeiros & Lebre 1992) derived spectroscopically indicates a large inclination angle ($i > 46°$) of the star's polar axis onto the line of sight. This effect contributes to explain the large rotational velocity of HD 223460 that is consistent with the hypothesis that the star is a normal G giant that has evolved from a single B type progenitor.

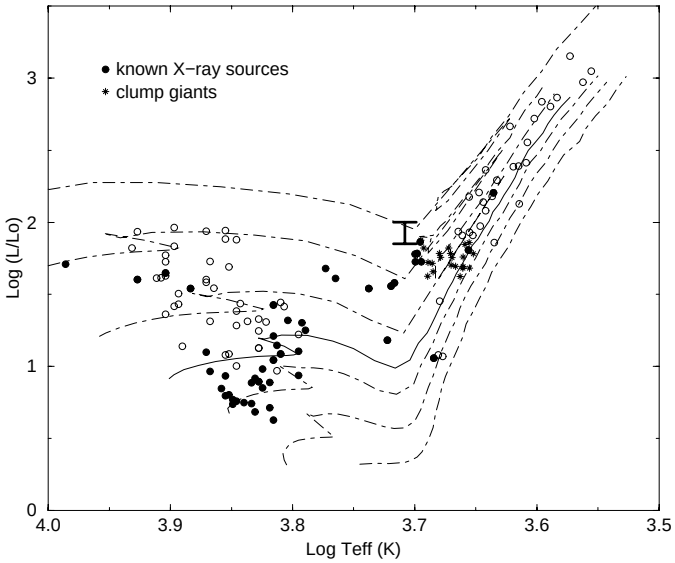

Fig. 1. H–R diagram of single giants (Gondoin 1999) compared with evolutionary tracks (Schaller et al. 1992). The dot-dashed lines from bottom to top describe the evolutionary tracks of 1 $M_\odot$, 1.25 $M_\odot$, 1.5 $M_\odot$, 2 $M_\odot$, 2.5 $M_\odot$ and 3 $M_\odot$ stars, respectively. The solid line is the evolutionary track of a 1.7 $M_\odot$ star. Open circles mark the H–R diagram positions of single field giants. Black circles mark giants known as X-ray sources. The H–R diagram location of HD 223460 is indicated by an error bar.

3. Observations and data reduction

HD 223460 was observed twice by the *XMM–Newton* space observatory (Jansen et al. 2001), in revolutions 107 on 9 July 2000, and 200 on 10 January 2001 (see Table 2). The satellite observatory uses three grazing incidence telescopes which provide an effective area higher than 4000 cm^2 at 2 keV and 1600 cm^2 at 8 keV (Gondoin et al. 2000). Three CCD EPIC cameras (Strüder et al. 2001; Turner et al. 2001) at the prime focus of the telescopes provide imaging in a 30 arcmin field of view and broadband spectroscopy with a resolving power of between 10 and 60 in the energy band 0.3 to 10 keV. Two identical RGS reflection grating spectrometers behind two of the three X-ray telescopes allow higher resolution ($E/\Delta E$ = 100 to 500) measurements in the soft X-ray range (6 to 38 Å or 0.3 to 2.1 keV) with a maximum effective area of about 140 cm^2 at 15 Å (den Herder et al. 2001).

HD 223460 observations were conducted with the EPIC cameras operating in full frame mode (Ehle et al. 2001). RGS spectra were recorded simultaneously. "Thick" aluminium filters were used in front of the EPIC MOS cameras and "Medium" thickness aluminium filters were used in front of EPIC p−n cameras to reject visible light. Processing of the raw event dataset was performed using the "emchain", "epchain" and "rgsproc" pipeline tasks of the *XMM–Newton* Science Analysis System (SAS version 5.3.0). HD 223460 spectra were built from photons detected within windows of about 60″ diameter around the target boresight in the EPIC cameras. The background was estimated on the same CCD chips as the source, within windows of similar sizes which were offset from the source position in an empty field region. The Pulse-Invariant (PI) spectra were rebinned such that each resulting MOS channel had at least 20 counts per bin and each p−n channel had at least 40 counts per bin. χ^2 minimization was used for spectral fitting. All fits were performed using the XSPEC package (Arnaud & Dorman 2001). The EPIC and RGS response matrices were generated by the SAS task "rmfgen" and "rgsrmfgen" respectively. EPIC p−n, MOS 1 and MOS 2 spectra were fitted together in the 0.3 to 9 keV energy range in revolution 107 and in the 0.3 to 6.5 keV energy range in revolution 200. The upper cut-off of the spectral band

Table 2. HD 223460 observation log during *XMM–Newton* revolutions 107 and 200.

Obs.	Experiment	Filter	Mode	Start Exp. (UT)	Exp. Duration
	MOS1	Thick	Prime Full	9 July 2000 @ 19:55:54	9094 s
	MOS2	Thick	Prime Full	9 July 2000 @ 19:55:54	9094 s
Rev. 107	p−n	Thick	Prime Full	9 July 2000 @ 20:02:13	6698 s
	RGS1		Spec + Q	9 July 2000 @ 20:03:50	10154 s
	RGS2		Spec + Q	9 July 2000 @ 20:03:50	10154 s
	MOS1	Thick	Prime Full	10 January 2001 @ 17:37:29	5994 s
	MOS2	Thick	Prime Full	10 January 2001 @ 17:37:29	5994 s
Rev. 200	p−n	Thick	Prime Full	10 January 2001 @ 17:43:46	3598 s
	RGS1		Spec + Q	10 January 2001 @ 17:43:45	6954 s
	RGS2		Spec + Q	10 January 2001 @ 17:43:45	6954 s

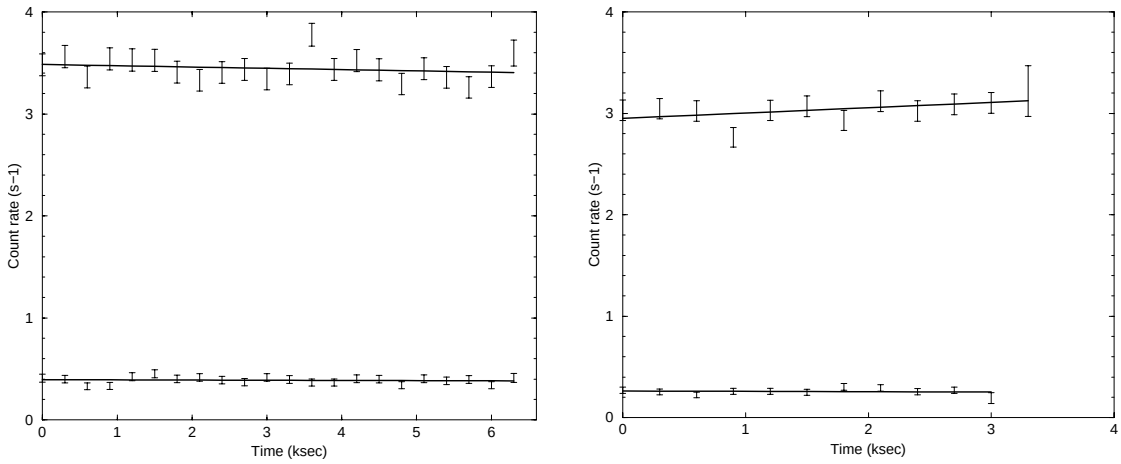

Fig. 2. Light curves of HD 223460 during revolutions 107 (left) and 200 (right) obtained with the EPIC p−n camera. In each graph, the upper curve is the count rate within the 0.3 to 2 keV band and the lower curve is the count rate within the 2 to 10 keV band. The events are binned in 300 s time intervals and the background contribution has been subtracted.

was imposed by the decreasing count rate at high energies. The RGS spectra were analysed separately due to their higher spectral resolution in the 0.3−2.1 keV energy range.

4. Integrated flux and temporal behaviour

Figure 2 shows the light curves of HD 223460 obtained during revolution 107 and 200 with the p−n camera after subtraction of background events. In the 0.3–2 keV energy band, the count rate is about 15% higher in revolution 107 with an average count rate of 3.45 ± 0.12 s^{-1} compared with a count rate of 3.04 ± 0.11 s^{-1} in revolution 200. In the 2–10 keV energy band, the count rate is about 50% higher in revolution 107 with an average count rate of 0.39 ± 0.03 s^{-1} compared with a count rate of 0.26 ± 0.06 s^{-1} in revolution 200. The 0.3–2 keV over 2–10 keV count rate ratios are 9 ± 1 and 13 ± 4 during revolutions 107 and 200 respectively, indicating that the spectrum of HD 223460 was soft during both observations. The count rate in the low energy band decreased steadily by ≈2.3% over 6.7 ksec in revolution 107. It increased steadily by about 5.6% over 1 hour in revolution 200.

The spectral analyses of each observation were conducted separately. Spectral fitting of the EPIC data (see Sect. 5.1) during these two periods yields flux measurements in the 0.3−2 keV and >2 keV bands. These measurements were converted into X-ray luminosities $L_{0.3-2\ \mathrm{keV}}$ and $L_{>2\ \mathrm{keV}}$ using Hipparcos parallax (π = 7.41 mas; ESA 1997). The luminosities are given in Table 3 which also provides the hardness ratio *hr* of the X-ray emission defined as $hr = (L_{>2\ \mathrm{keV}} - L_{0.3-2\ \mathrm{keV}})/(L_{>2\ \mathrm{keV}} + L_{0.3-2\ \mathrm{keV}})$. Table 3 confirms that the X-ray spectrum of HD 223460 is soft. Compared with revolution 200, the X-ray luminosity of HD 223460 during revolution 107 was 19% higher in the 0.3–2 keV band and about 46% higher in the >2 keV energy band.

Table 3. X-ray luminosities (corrected for interstellar absorption) of HD 223460 in the 0.3−2 keV and 2−10 keV measured with the combined EPIC MOS and pn cameras. The percentage contribution in luminosity of hot plasmas ($kT > 1$ keV) is indicated between bracketts. The hardness ratio (*hr*) is defined as $hr = (L_{>2\ \mathrm{keV}} - L_{0.3-2\ \mathrm{keV}})/(L_{>2\ \mathrm{keV}} + L_{0.3-2\ \mathrm{keV}})$.

Obs.	$L_{0.3-2\ \mathrm{keV}}$ (10^{30} erg s^{-1})	$L_{>2\ \mathrm{keV}}$ (10^{30} erg s^{-1})	*hr*
Rev. 107	27.0 (78%)	10.7 (98%)	–0.43
Rev. 200	22.7 (78%)	7.3 (98%)	–0.51

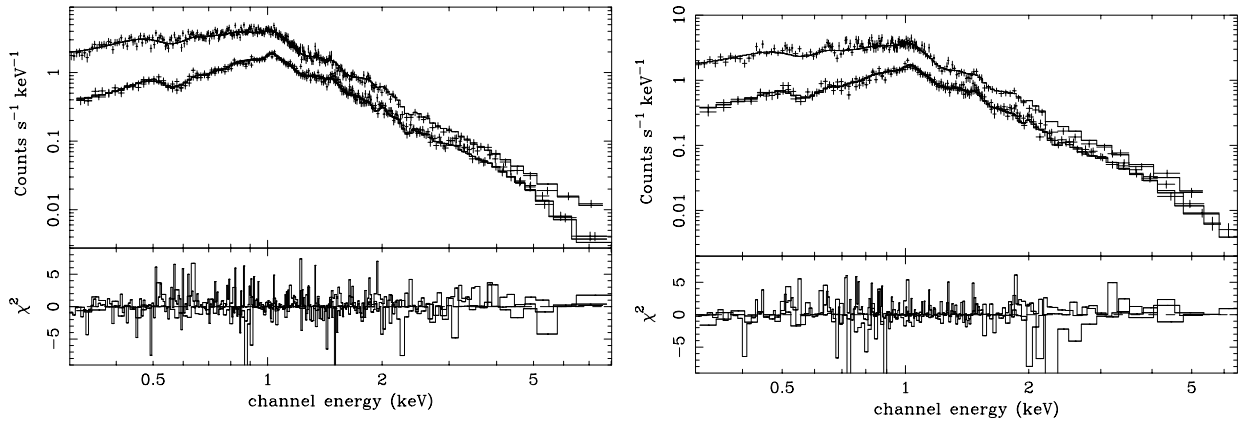

Fig. 3. Best fit models to revolution 107 (left) and revolution 200 (right) EPIC spectra. The data (crosses) and spectral fit (solid line) to the EPIC pn (upper curve) and EPIC MOS (lower curve) spectra are shown in the upper panel. The χ^2 contributions are given in the lower panel of each graph.

Table 4. Best fit parameters to EPIC data using a 2 components MEKAL model (Mewe et al. 1985) with variable abundance and a variable hydrogen column density.

	Rev. 107	Rev. 200
Z	0.32 ± 0.02	0.28 ± 0.03
kT_1 (keV)	0.73 ± 0.09	0.74 ± 0.01
EM_1 (10^{52} cm^{-3})	62 ± 6	61 ± 9
kT_2 (keV)	2.10 ± 0.03	1.78 ± 0.04
EM_2 (10^{52} cm^{-3})	258 ± 1	219 ± 7
χ^2	855/749 d.o.f. = 1.14	615/541 d.o.f. = 1.14

Table 5. Best fit parameters to EPIC data using a 3 components MEKAL model (Mewe et al. 1985) with variable abundance and a variable hydrogen column density.

	Rev. 107	Rev. 200
Z	0.21 ± 0.02	0.20 ± 0.03
kT_1 (keV)	0.65 ± 0.02	0.66 ± 0.03
EM_1 (10^{52} cm^{-3})	72 ± 10	62 ± 18
kT_2 (keV)	1.38 ± 0.06	1.34 ± 0.08
EM_2 (10^{52} cm^{-3})	197 ± 29	190 ± 54
kT_3 (keV)	3.7 ± 0.6	3.6 ± 1.6
EM_3 (10^{52} cm^{-3})	102 ± 32	60 ± 60
χ^2	743/747 d.o.f. = 0.99	570/539 d.o.f. = 1.06

5. Spectral analysis

5.1. Analysis of EPIC data

The two EPIC datasets (see Fig. 3) were fitted separately with the MEKAL optically thin plasma emission model (Mewe et al. 1985). The spectral fitting was performed in the 0.3–9 keV and 0.3–6.5 keV spectral bands for revolutions 107 and 200, respectively since revolution 200 data does not contain any significant signal above 6.5 keV. The interstellar hydrogen column density was left free to vary. $N_{\rm H}$ values in the range (3.1–5.4) $\times$ 10^{20} cm^{-2} were derived from the analysis of the two datasets which are lower than the total galactic H I column density $N_{\rm H}$ = 8.0 $\times$ 10^{20} cm^{-2} (Dickey & Lockman 1990) in the direction of HD 223460. No single temperature plasma model that assumes either solar photospheric (Anders & Grevesse 1989) or non solar abundances can fit the data, as unacceptably large values of χ^2 were obtained. The MEKAL plasma models with two components at different temperatures prove adequate for the two datasets (see Table 4). The coronal emission measure distribution has been proposed to be double peaked for many stars (Schrijver et al. 1995; Mewe et al. 1996; Güdel et al. 1997a, 1997b). In particular, best fit MEKAL models to *ROSAT* data obtained in January 1993 (Singh et al. 1996) suggests a coronal plasma in HD 223460 with two components at distinct temperatures. Different models could produce acceptable fits to the *ROSAT* PSPC spectra, some of which with best fit temperatures similar to those derived from EPIC data.

As spatially unresolved observations gain in spectral resolution and signal to noise ratio, the amount of details in the spectra of stellar coronae which must be reproduced increases reflecting the true complexity of the sources plasma. Multi-temperature models are now necessary to explain high-resolution spectra of stellar coronae (Dupree et al. 1993; Griffiths & Jordan 1998; Bowyer et al. 2000). Recent analysis of *XMM–Newton* and *Chandra* X-ray spectra find that a continuous emission measure distribution fits the data better and is more realistic physically (Audard et al. 2001a,b; Güdel et al. 2001; Mewe et al. 2001). Hence, we tried to fit the EPIC spectra of HD 223460 using a MEKAL model with three components at different temperatures and with the same metallicity. The improvement in χ^2 statistics compared with the two temperatures model ($\Delta\chi^2/\Delta\nu$ = 56 for 747 degrees of freedom and $\Delta\chi^2/\Delta\nu$ = 22 for 539 degrees of freedoms on the best fit to revolution 107 and 200 datasets, respectively) is significant to a >99% confidence level using the F-statistic. The "cool" component in the three component model has a slightly lower temperature but an emission measure similar to that given by the two component model. The three component model suggests that most of the emission measure of the "hot" plasma is located around T = 1.6$\times$$10^7$ K but with a significant contribution above T = 3$\times$$10^7$ K. The emission measure and temperature of this very hot plasma component are not well constrained. The temperatures of the different plasma components remain the

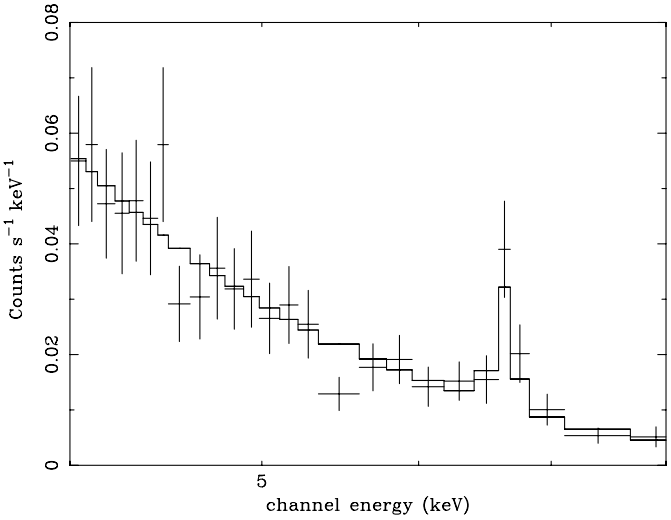

Fig. 4. Comparison of the EPIC pn spectrum of HD 223460 obtained during revolution 107 with a best fit power law + Gaussian model in the 3–9 keV range.

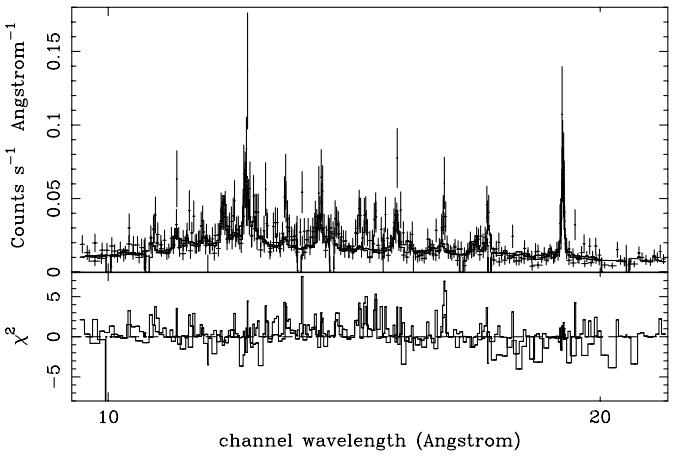

Fig. 5. Comparison of the RGS spectra of HD 223460 obtained during revolution 107 with a best fit VMEKAL model with 3 temperature components (see Table 6, model C) in the 10–25 Å range. The data (crosses) and spectral fit to the RGS spectra are shown in the upper panel. The χ^2 contributions are given in the lower panel.

same for revolution 107 and 200. Hot ($T > 1.6 \times 10^7$ K) plasma on HD 223460 is the main source of X-ray emission both in the soft and in the hard X-ray band. It contributes to 98% of the X-ray luminosity above 2 keV. Table 5 shows that the higher X-ray luminosity of HD 223460 in revolution 107 both in the soft and in the hard energy range is related to a higher emission measure of the hottest plasma. The average element abundance in HD 223460 corona is found to be lower than the solar photospheric value (see Tables 4 and 5). No significant variations of abundance are detected between the two revolutions.

One major feature of HD 223460 spectrum during revolution 107 is the presence of a high energy tail and of an emission feature around 6.6 keV attributed to an iron K emission line (see Fig. 4). This component is not detected in revolution 200 data. The iron Kα fluorescence line consists of two components Kα_1 and Kα_2 at 6.404 keV and 6.391 keV respectively for Fe I and a branching ratio of 2:1 (Bambynek et al. 1972). The natural width of the lines ($\Delta E \approx 3.5$ eV) and any broadening due to thermal motions of the emitting atoms ($\Delta E(\mathrm{eV}) \approx 0.4(T/10^6)^{1/2}$) are negligible compared to the energy resolution (155 eV FWHM) of the EPIC cameras. The iron Kα fluorescent line energy is an increasing function of the ionization state. It rises slowly from 6.40 keV in Fe I to 6.45 keV in Fe XVII (neon-like) and then increases steeply with the escalating number of vacancies in the L-shell to 6.7 keV in Fe XXV and 6.9 keV in Fe XXVI (House 1969; Makishima 1986). Spectral fits to the EPIC p−n spectra above 3 keV by a powerlaw and a Gaussian line model give a power law with a slope $\Gamma = 3.0 \pm 0.3$ and an Fe K line at 6.65 ± 0.06 keV with an equivalent width $EW \approx 400 \pm 70$ eV and a flux $f_X \approx 10^{-13}$ erg cm^{-2} s^{-1}. The improvement of the power law fit with an additional Gaussian line is significant ($\Delta\chi^2/\Delta\nu = 6$ for 32 degrees of freedom) to a >95% confidence level using the F-statistic. This result indicates the presence of iron in high Fe XXV states of ionization during revolution 107. For a collisionally dominated optically thin coronal plasma, the Fe XXV ion concentration reaches a maximum value in the $2-7 \times 10^7$ K temperature range (Raymond-Smith 1977), in agreement with the temperature of the hot plasma component derived by spectral fitting. This supports the thermal origin of the Fe K emission.

Among all of the different changes, eruption and instabilities which are seen on the Sun, the ones which are labeled "flares" all have in common material heated to temperatures of 10^7 K or higher (Golub & Pasachoff 1997; Reale et al. 2001). Such temperatures are not seen in the non-flaring corona, and events which do not produce such hot plasma do not seem to be called flares. The emission measure of some active stellar coronae has two peak, one at at a few 10^6 K and the other around 10^7 K, and it has been proposed that the higher temperature peak is due to continuous flaring activity (Drake et al. 2000; Sanz-Forcada et al. 2002). However, such a flaring activity is expected to induce count rate fluctuations that are not observed in the EPIC light curves of HD 223460. Hence, also suggestive, the existence of significant amounts of 10^7 K material and the detection of Fe XXV emission cannot be regarded as a proof for the presence of flares in the corona of HD 223460.

5.2. Analysis of RGS data

The low energy RGS spectra were fitted with a VMEKAL model with three components at different temperatures. The VMEKAL model generates a spectrum of hot diffuse gas with line emission from several elements based on the calculation of Mewe et al. (1985) with Fe L calculations by Liedahl (1995). Hence, three electron temperatures and electron densities are assumed for the entire ensemble of element charge states and in particular for iron, oxygen and neon which produce the most prominent lines. This assumption turns out to be fairly adequate within the observational uncertainties of the present spectrum (see Fig. 5). The fit was performed in the spectral range from 9.5 Å to 25 Å where the efficiency of the RGS spectrometers is the highest. The model temperatures of the cool, mid-temperature and hot plasma components were frozen to

Table 6. Best fit parameters to RGS spectra in the 0.5–1.3 keV range recorded in revolutions 107 (upper table) and 200 (lower table) using a three components VMEKAL model. The temperature of each component were frozen to the value derived from the analysis of EPIC data (see Table 5). The metallicity was left free to vary. The oxygen and neon abundances were first tied to the abundance of the other elements (MODEL A). There were then left free to vary independently but with the same value for the different temperature components (MODEL B). In MODEL C, the hottest temperature component has been replaced by a VMEKAL component at 4×10^6 K where the Ne IX line is formed.

Rev.107	Parameter	MODEL A	MODEL B	MODEL C
	kT_1 (keV)	0.65	0.65	0.65
	EM_1 (10^{52} cm^{-3})	57 ± 17	52 ± 13	41 ± 15
	kT_2 (keV)	1.38	1.38	1.38
	EM_2 (10^{52} cm^{-3})	366 ± 44	342 ± 41	399 ± 13
VMEKAL	kT_3 (keV)	3.7	3.7	0.34
	EM_3 (10^{52} cm^{-3})	85 ± 68	81 ± 65	55 ± 15
(3 components)	O	0.11	0.18 ± 0.03	0.10 ± 0.01
	Ne	0.11	0.52 ± 0.09	0.35 ± 0.05
	Other abundances	0.11 ± 0.03	0.11 ± 0.02	0.11 ± 0.01
	χ^2	1.33 (549/413 d.o.f.)	1.24 (509/411 d.o.f.)	1.14 (469/411 d.o.f.)
Rev.200	Parameter	MODEL A	MODEL B	MODEL C
	kT_1 (keV)	0.66	0.66	0.66
	EM_1 (10^{52} cm^{-3})	78 ± 24	81 ± 65	72 ± 26
	kT_2 (keV)	1.34	1.34	1.34
	EM_2 (10^{52} cm^{-3})	364 ± 63	320 ± 65	351 ± 26
VMEKAL	kT_3 (keV)	3.6	3.6	0.34
	EM_3 (10^{52} cm^{-3})	0–146	0–163	0–46
(3 components)	O	0.11	0.10 ± 0.03	0.08 ± 0.03
	Ne	0.11	0.44 ± 0.12	0.37 ± 0.10
	Other abundances	0.11 ± 0.01	0.11 ± 0.01	0.11 ± 0.01
	χ^2	0.75 (167/223 d.o.f.)	0.69 (153/221 d.o.f.)	0.70 (156/221 d.o.f.)

the values derived from EPIC data (see Table 5). The abundances of the O and Ne elements which give prominent lines in the considered spectral range were first tied to the abundance of the other elements (MODEL A). They were then allowed to vary independently but with the same value for all temperature components (MODEL B). In a third model (MODEL C), the hottest temperature component has been replaced by a VMEKAL component at 4×10^6 K where the Ne IX line is formed. Fitting results are given in Table 6. The photon statistics in the RGS spectra of revolution 200 is lower than in the revolution 107 dataset. The fit supports the three components plasma model for the interpretation of the EPIC and RGS data. The emission measures of low and hot temperature components are similar to the values derived from the analysis of EPIC spectra (see Table 5). However, the emission measure of the mid-temperature component in RGS is higher ($EM \approx 350 \times 10^{52}$ cm^{-3}) than the value derived from EPIC data ($EM \approx 200 \times 10^{52}$ cm^{-3}) as suggested by the line flux measurements (see Table 7). When left free to vary, the oxygen abundance is similar to the average abundance of the other elements. The determination of abundances relative to hydrogen requires an accurate measurement of the X-ray continuum which cannot be reliably measured even from the RGS spectra (see Fig. 5) due to their moderate spectral resolution and signal to noise ratio. Therefore it is modeled from the flux left over when all of the known emission lines in the VMEKAL model are included. However, no plasma spectroscopy code includes all of the emission lines, so the missing weak emission lines are misinterpreted as continuum flux (Schmitt et al. 1996), thereby raising the hydrogen abundance derived from the free-free continuum and lowering all of the metal abundances relative to hydrogen. This systematic error in the metal abundances relative to hydrogen is not included in the abundance uncertainties stated in Table 6 but the fitting results suggest that neon abundance of the hot plasma component is significantly higher than the oxygen abundance. The improvement in χ^2 fit statistics ($\Delta\chi^2/\Delta\nu = 20$ for 411 degrees of freedom and $\Delta\chi^2/\Delta\nu = 10$ for 221 degrees of freedom, respectively for revolution 107 and 200) induced with variable O and Ne abundance is significant at >99% confidence using the F-statistic. Hence, the Ne/O ratio found for HD 223460 seems higher than in the solar photosphere. This indication of a Ne abundance enhancement is reminiscent of a similar anomaly observed in a subset of solar flares (Murphy et al. 1991; Schmelz 1993). Large Ne abundance enhancements are a common feature of active stellar coronae (Güdel et al. 2001; Huenemoerder et al. 2001) and an inverse FIP effect is observed in very active coronae (Brinkman et al. 2001; Drake et al. 2001) where the abundances (relative to oxygen) increase with increasing first ionization potential (FIP).

Figure 6 shows the RGS spectra of HD 223460 averaged over revolution 107 and 200. Each spectrum is the sum of the two spectra simultaneously obtained with the RGS1 and RGS2 reflection grating spectrometers on board *XMM–Newton*. Line fluxes and positions were measured using the XSPEC package by fitting simultaneously the RGS1 and RGS2 spectra with a sum of narrow Gaussian emission lines convolved with the response matrices of the RGS instruments. The continuum emission was described using bremsstrahlung models with temperatures frozen to the best fit values derived

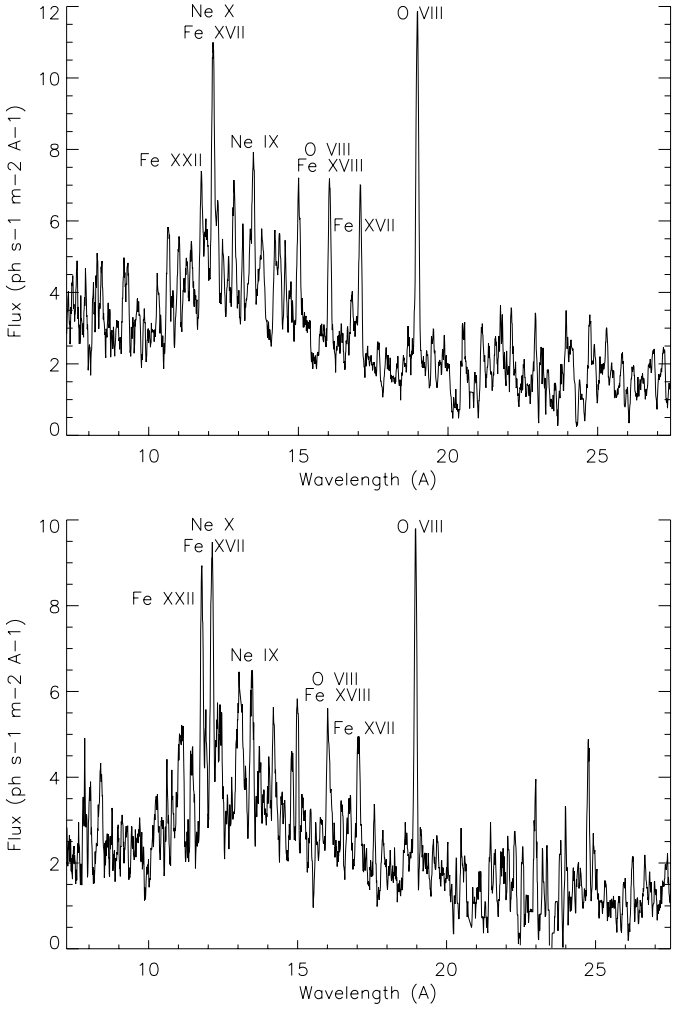

Fig. 6. Averaged first order spectra of RGS 1 and 2 obtained during revolutions 107 (top) and 200 (bottom).

by spectral fitting (see Table 6; MODEL C). The strong lines were included in the fit, so the continuum of the weaker lines is better evaluated. For line identification, we required only that the wavelength coincidence be comparable to the spectral resolution of the RGS spectrometers, namely 0.04 Å over the 5 to 35 Å wavelength range. In the X-ray domain, several candidate lines may exist within this acceptable wavelength coincidence range. Hence, we only looked for resonance transitions of abundant elements, and predicted line intensities using spectra of the Sun (Doschek & Cowan 1984) and of Capella (Brinkman et al. 2000). Series of lines of highly ionized Fe and several lines of the Ly and He series are visible in RGS spectra, most notably from O and Ne. Estimates or upper limits of line fluxes are reported in Table 7. Their temperatures of maximum formation range between 3×10^6 K and 2×10^7 K suggesting that the corresponding ions are mainly associated with the cool plasma components inferred from EPIC data. However, lines such as the O VIII and Ne X lines have emissivity functions quite spread out in temperature to which material present in the hot component contributes too. Also, the Ne IX line indicates the presence of cooler material than the cool component reported. No significant line intensity variations are observed between revolutions 107 and 200. The Ne X (12.13 Å), Ne IX (13.45 Å) and Fe XIX (13.74 Å) lines are affected by blends. This could explain that their flux upper limits (see Table 7) are inconsistently high compared with the values expected from the analysis of EPIC spectra. Lines with low temperature ($T < 6 \times 10^6$ K) of maximum line formation give emission measures consistent with the values $EM \approx 60{-}70 \times 10^{52}$ cm^{-3} and $Z = 0.2$ of the EPIC low temperature plasma component (see Table 5). The Fe XVIII (14.56 Å) and Fe XXII (11.79 Å) lines whose temperature of maximum formation is greater than 6×10^6 K give emission measures higher than the value $EM \approx 200 \times 10^{52}$ cm^{-3} of the EPIC mid-temperature plasma component (see Table 5). This is likely due to uncertainties in their flux determination although effects related to the cross-calibration accuracy between EPIC and RGS are not excluded.

The emitting volume of the different plasma components could be constrained if their electron densities were known. These can be measured using density-sensitive spectral lines originating from meta-stable levels, such as the forbidden $(f)2^3S{-}1^1S$ line in helium-like ions. This line and the associated resonance $(r)2^1P{-}1^1S$ and inter-combination (i) $2^3P{-}1^1S$ lines make up the so-called helium-like triplet lines (Gabriel & Jordan 1969; Pradhan 1982). The intensity ratio $(i + f)/r$ varies with electron temperature and the ratio i/f varies with electron density due to the collisional coupling between the meta-stable 2^3S upper level of the forbidden line and the 2^3P upper level of the inter-combination line. The RGS wavelength band contains the He-like triplets from O VII, Ne IX, Mg XI and Si XIII. However, the Si, Mg and O triplets are not detected in the RGS spectra of HD 223460 and the Ne IX triplet is too heavily blended with iron and nickel lines for density analysis.

6. Discussion

6.1. Structure of HD 223460 corona

The spectral fitting of the EPIC and RGS spectra of HD 223460 suggests a corona configuration with little contribution from quiet regions similar to the Sun. On the contrary the temperature $T \approx 7.5 \times 10^6$ K of the "cool" plasma component is reminiscent of solar type active regions, while the hot ($T > 10^7$ K) component may be caused by disruptions of magnetic fields associated to a permanent flaring activity. The review of coronal activity by Vaiana & Rosner (1978) pointed out that the Sun, if completely covered with active regions, would have an X-ray luminosity of 2×10^{29} ergs s^{-1}. When scaled to the surface of HD 223460 ($R \approx$ 10–13 $R_\odot$; see Table 1), an X-ray luminosity of about $(2.0{-}3.4) \times 10^{31}$ erg s^{-1} is obtained. This value is comparable with the observed X-ray luminosity of HD 223460 ($(3{-}4) \times 10^{31}$ erg s^{-1}) derived using Hipparcos parallaxes. It is higher than the X-ray luminosity contribution ($\approx (5.1{-}6.2) \times 10^{30}$ erg s^{-1}) of its "cool" ($T \approx 7.5 \times 10^6$ K) plasma component. The X-ray luminosity of the "cool" plasma component could be explained if 15–31% of the surface of HD 223460 is covered with bright solar like active regions. Assuming that these active regions can be described by a simple static loop system consisting of similar loops of constant pressure p (dyn cm^{-2}), temperature T (K) and cross

Table 7. Measured positions and flux estimate or upper limits of the strongest lines in the RGS spectra of HD 223460 obtained during revolutions 107 and 200. The columns give the predicted line positions, the measured line positions during revolution 107, the measured line positions during revolution 200, the ion and line identifications, the temperatures of maximum line formation, the line fluxes measured during revolution 107 and the line fluxes measured during revolution 200.

$\lambda_{\rm pred}$ (Å)	$\lambda_{\rm rev107}$ (Å)	$\lambda_{\rm rev200}$ (Å)	Ion	line ID	$\log(T_{\rm m})$ log (K)	$F_{\rm rev107}$ (10^{-6} cm^{-2} s^{-1})	$F_{\rm rev200}$ (10^{-6} cm^{-2} s^{-1})
11.79	11.68	11.68	Fe XXII		7.10	42 ± 26	<70
12.13	12.17	12.17	Ne X	H1AB	6.80	162 ± 35	110 ± 53
12.12			Fe XVII	4C	6.75		
13.45	13.55	13.55	Ne IX	He4w	6.60	71 ± 29	52 ± 46
13.46			Fe XIX		6.90		
13.50			Fe XIX		6.90		
13.74	13.74	13.74	Fe XIX		6.90	81 ± 34	45 ± 40
13.78			Ni XIX		6.70		
14.56	14.56	14.56	Fe XVIII	F10	6.80	50 ± 26	<54
16.01	16.01	16.01	O VIII	H2	6.60	62 ± 31	65 ± 38
16.07			Fe XVIII	F3	6.80		
16.78	16.78	16.78	Fe XVII	3F	6.70	33 ± 29	<61
17.05	17.05	17.05	Fe XVII	3G	6.70	58 ± 35	49 ± 45
17.10			Fe XVII	M2	6.70		
18.97	18.97	18.97	O VIII	H1AB	6.50	100 ± 41	89 ± 52

section A (cm^2), the emission measure EM (cm^{-3}) of the "cool" plasma can be expressed as:

$$EM = GF \times (4\pi R^2) \times \left(\frac{p}{2kT}\right)^2 \times L \quad (1)$$

where R is the stellar radius, F is the filling factor and L the loop half-length. G is a geometry factor which includes effect of partial occultation of the corona by the star itself (i.e. G varies from 0.5 to 1 for $L << R$ to $L >> R$). Using the relation $T = 1400 \times (pL)^{1/3}$ (Rosner et al. 1978) and $G = 0.7$, a characteristic loop length scale is obtained (Mewe et al. 1982):

$$L_{10} = 7.4F \times T_7^4 \times EM_{52}^{-1} \times (R/R_\odot)^2 \quad (2)$$

where L_{10} is the loop half length in units of 10^{10} cm, T_7 is the coronal temperature in unit of 10^7 K, and EM_{52} is the emission measure in units of 10^{52} cm^{-3}. Inserting the observed temperature and emission measure of the cool plasma component (see Table 5) and $R = 12\ R_\odot$ (see Table 1), we find $L \approx 1.0 \times 10^{10}$ cm^{-3} assuming a ≈20% filling factor for revolution 107 and 200 (see Table 8). The pressure scale height H (in cm) is given by $H = 5 \times 10^3 \times T \times (g/g_\odot)^{-1}$ where $g/g_\odot$ is the surface gravity expressed in solar units and T the temperature in Kelvin. For HD 223460, $g/g_\odot = 0.022$ using $M = 2.95\ M_\odot$ and $R = 11.5\ R_\odot$ (see Table 1). Since it turns out that the loop lengths are much smaller than the pressure scale height H, the assumption of constant pressure in the loops is justified. Characteristic loop size and temperature on HD 223460 are respectively 10^{10} cm and 7.5×10^6 K. Solar corona observations by comparison show bright hot loops within active regions which reach maximum temperatures and electron densities above the neutral line of typically (3–4) $\times 10^6$ K and 10^{10} cm^{-3} (Vaiana et al. 1973). In addition to these hot loops, on-disk images of the Sun show that neighbouring active regions are often connected into complexes of activity by large loop-like structures (van Speybroek et al. 1970). Such interconnecting loops can be $>10^{10}$ cm long, i.e. as long as the loop length estimate on HD 223460. However, they tend to be cooler than loops within solar active regions and therefore cooler than coronal loops on HD 223460.

Table 8. Physical parameters of HD 223460 coronal loops derived from the *XMM–Newton* observations conducted during revolution 107 and 200. The electron density is derived from Eq. (1), i.e. $n_{\rm e} = 2 \times \sqrt{EM/(4\pi \times GF \times R^2 \times L)}$.

	T (K)	EM (cm^{-3})	H (cm)	L (cm)	$n_{\rm e}$ (cm^{-3})
Rev. 107	7.5×10^6	72×10^{52}	171×10^{10}	0.9×10^{10}	1.7×10^{10}
Rev. 200	7.7×10^6	62×10^{52}	175×10^{10}	1.2×10^{10}	1.3×10^{10}

If, in HD 223460, the cool plasma components is produced by solar like active regions covering a large fraction of the star's surface, it is easy to imagine that such a dense population of active regions coexists with constant interaction and disruption of their magnetic fields which might be expected to lead to continuous flaring. This could explain the permanent emission measure of hot plasma above 10^7 K. High temperature plasmas have been detected from the Sun and from non-solar coronae (van den Oord & Mewe 1989; Tsuru et al. 1989). The solar flare plasma shows a bimodal temperature distribution with plasma at two different temperature (4–8) $\times 10^6$ K and (16–26) $\times 10^6$ K where the hot component is present only during the flares (Antonucci & Dodero 1995). The two components probably have a common origin in the flaring region on the Sun. It is worth noting that the temperature of these components are close to the plasma temperatures derived from the spectral analysis of HD 223460 X-ray emission. There is evidence that the emission measure distribution of very active

stellar coronae, obtained from spectrally resolved XUV observations, is double-peaked. A study of the transition regions and coronae of the RS CVn binaries V711 Tau, AR Lac and II Peg (Griffiths & Jordan 1998) indicates the existence of two distinct peaks in the high temperature emission measure distribution around 6.3×10^6 K and 20×10^6 K. Recently, Sanz-Forcada et al. (2002) derived the emission measure distribution of a sample of RSCVn binaries and single active stars including the low-rotation giant β Cet. They noticed that emission measure distributions are remarkably similar among all the stars, showing a narrow enhancement or bump around $\log T_e \approx 6.9$. This aspect is much debated and still open, but it has been suggested that this hot component may be due to a continuous flaring activity (Güdel 1997; Drake et al. 2000). The surface of active stars is covered by active regions, and flares would be so frequent that their light curves overlap, canceling out any variability due to single events. Reale et al. (2001) showed that a double-peaked emission measure distribution is obtained if one combines the $EM(T)$ of the whole solar corona with the envelope of the $EM(T)$ profiles during solar flares. This seems to suggest that uninterrupted sequence of overlapping proper flares, whichever their evolution, could produce a double peak emission measure distribution in the coronae of active stars. This could explain the presence of hot coronal material even in the absence of obvious flares. There could be small-scale flares not well identified in the light curve of XUV data with moderate signal-to-noise ratio. Within this interpretation, the higher emission measure and luminosity contribution of the hot plasma component in revolution 107 would be related to a more intense flaring activity of HD 223460 in July 2001. On the other hand, the steady flux decrease during revolution 107 and flux increase during revolution 200 could be interpreted as the gradual disappearance or emergence of active regions at the limb of the star. Since active regions might not be homogeneously distributed on the surface of the star, it is difficult with the presented data to distinguish between a long-term variability of the flaring activity and a rotational modulation of the X-ray emission by long lived active regions.

6.2. Evolution of HD 223460 corona

One hypothesis regarding HD 223460 origin (see Sect. 2) is that the star originates from a single, early B-type star as it evolves in the giant domain, crosses the Hertzsprung gap and becomes a convective late-type giant. To be likely, this scenario should account for the photometric period of the star ($P_{\rm phot} \approx 23$ days; Strassmeier & Hall 1988) and for the recent estimate ($v_{\rm eq} \approx 25$ km s^{-1}; see Table 1) of its equatorial velocity. We compared this value with $v \sin i$ values of A-F giants extracted from the Bright Star Catalogue and with $v \sin i$ measurements of G-K giants obtained with CORAVEL by de Medeiros & Mayor (1995). The CORAVEL measurements are precise to about 1 km s^{-1}. All projected equatorial velocity measurements are plotted in Fig. 7 as a function of $T_{\rm eff}$ for different mass ranges. A-F giants ($T_{\rm eff} > 6000$ K) have high rotational velocities, often greater than 100 km s^{-1}. K giants, on the contrary, have low $v \sin i$ values of 1 or 2 km s^{-1}

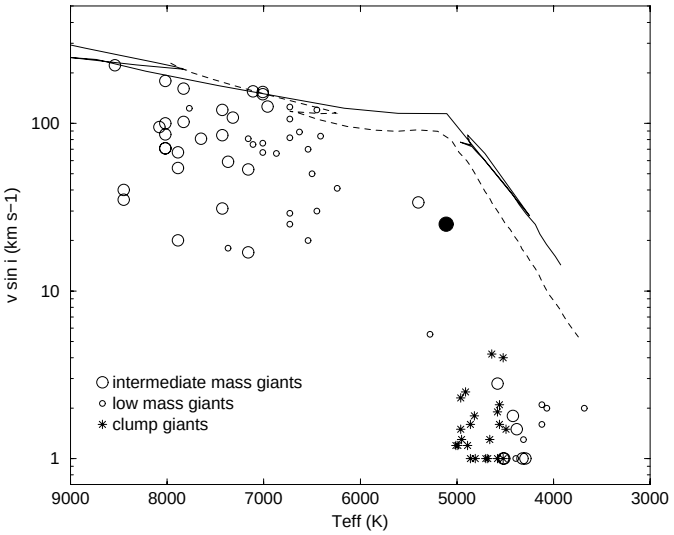

Fig. 7. Equatorial rotational velocity of HD 223460 (filled circle) compared with $v \sin i$ values of single field giants (Gondoin 1999). The solid line and the dashed line describe the equatorial velocity evolution of 1.7 $M_\odot$ and 2.5 $M_\odot$ stars respectively assuming angular momentum conservation and $v \sin i = 150$ km s^{-1} at $T_{\rm eff} = 7000$ K.

for $T_{\rm eff} < 4700$ K. As noticed by Simon & Drake (1989), stellar rotation strongly decline during the rapid evolution of G giants across the Hertzsprung gap. These authors also suggested, along with Gray (1989), that magneto-hydrodynamic braking due to stellar winds could explain this phenomenon. Rutten & Pylyser (1988) argued that during the entire evolution of a 3 $M_\odot$ star the timescale for magnetic braking is larger than the evolutionary time scale. Endal & Sofia (1979) and Gray & Endal (1982) pointed out that the expansion of the stars on the red giant branch together with the rearrangement of angular momentum due to the increasing depth of the convection zones may well explain the decrease of $v \sin i$ for cool giants. Gondoin et al. (2002) calculated the equatorial velocity evolution of 2.5 $M_\odot$ giants using Schaller et al. (1992) evolutionary models and assuming angular momentum conservation and $v \sin i = 150$ km s^{-1} at $T_{\rm eff} = 7000$ K. Comparisons with $v \sin i$ measurements (see Fig. 7) confirm that angular momentum conservation alone cannot explain the rotational velocities of K giants. However, Fig. 7 suggests that HD 223460, which is located near the bottom of the RGB, just starts experiencing rotational braking. Most of its angular momentum could have been conserved within its convective envelope during its rapid evolution from mid-F spectral type. Evolution from an early B type star with a moderate rotation velocity could then explain the current rotation period of the star.

Within this hypothesis, the outer convection zone of HD 223460 would have deepened since its formation at mid-F spectral type, thus increasing the convective turnover time scale (Gilliland 1985). Since HD 223460 only experienced a small spin down (see Fig. 7) and maintained a relatively high rotation rate, the Rossby number (Durney & Latour 1978) decreased and dynamo activity increased as the star evolved towards the bottom of the RGB. During this period, the deepening convective envelope likely suffered shear stresses,

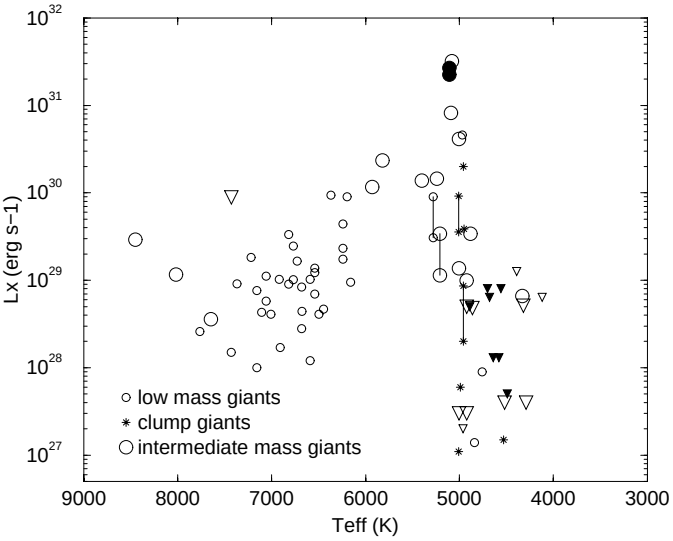

Fig. 8. *XMM–Newton* luminosities of HD 223460 (filled circles) in the 0.3 to 2 keV band compared with ROSAT PSPC measurements of single field giants (Hünsch et al. 1998; Pizzolato et al. 2000). Upper limits of X-ray luminosities measured with the Einstein (Maggio et al. 1990) and ROSAT (Pizzolato et al. 2000) observatories are indicated by small triangles, large triangles and filled triangles for low-mass ($1.2\ M_\odot < M < 2.0\ M_\odot$), intermediate- mass ($2.0\ M_\odot < M < 2.5\ M_\odot$) and clump giants respectively.

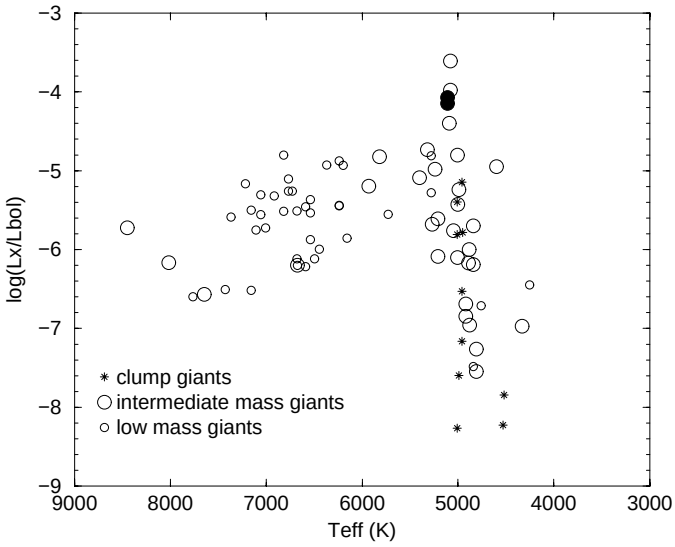

Fig. 9. Ratio of the X-ray to bolometric luminosities of HD 223460 (filled circles) in the 0.3 to 2 keV band compared with single field giants (Hünsch et al. 1998; Gondoin 1999; Pizzolato et al. 2000).

which could have resulted in radial velocity gradients. The necessary conditions were then present to switch on an α-Ω dynamo with an increasing efficiency as the star evolved towards the bottom of the RGB. Our spectral analysis of the X-ray data suggests that the fluid kinetic helicity induced by the rotation currently generates magnetic fields with characteristic scale of 10^{10} cm, i.e. comparable with large interconnecting solar loops. The dynamo productive of large magnetic flux induces a high density of active regions covering up to 30% of the star surface. We argue that the X-ray emission is strongly enhanced due not only to the occurrence of these large scale magnetic structures, but also to their permanent interactions. These interactions would lead to an uninterrupted flaring activity that generates a large volume of hot plasmas. Since HD 223460 could be soon ascending the RGB, it is anticipated that its rotation will spin down dramatically with the effect of increasing its Rossby number and decreasing its helicity-related dynamo-driven activity. Not only the rotational braking per se but also the restoration of rigid rotation could prevent the maintenance of large magnetic structures as the star ascends the red giant branch (Gondoin 1999). Rosner et al. (1995) pointed out that this suppression of a large-scale dynamo leads to the disappearance of large-scale organized stellar magnetic fields but does not imply the suppression of magnetic field production at small scale, driven by the turbulent motion in the surface convection zones. A bifurcation in magnetic loop sizes could occur as the dynamo induced by rotation gives way to a turbulent field generation mechanism like that described by Durney et al. (1993). According to this scenario, X-ray emission from large coronal loops and the related flaring activity should progressively disappear as HD 223460 evolves from G to K spectral type (see Fig. 8).

The above evolution scenario implies that, from the successive effects of convection zone deepening and rotational braking, a minimum value of the Rossby number is expected around HD 223460 evolutionary stage. At this stage, $\alpha - \Omega$ dynamo mechanisms (Parker 1955) should operate with maximum efficiency. Capella observations (Johnson et al. 2000) of the Fe XXI λ1354 formed at 10^7 K suggest a significant variability over the past 5 years in the hottest part of the corona of the G8 III primary thought to be a He-burning clump giant. This suggests that cyclic activity and strong variability are seen in late evolutionary stages. The positive effect of deepening convective envelope on coronal activity would allow even the slowly rotating new arrivals to the clump still to be somewhat active (Ayres et al. 1998). We compared our X-ray flux measurements of HD 223460 (see Sect. 4) in the 0.3 to 2 keV band with X-ray fluxes of single field giants extracted from the ROSAT all-sky survey catalogue (Hünsch et al. 1998). Upper limits of *Einstein* X-ray fluxes were also retrieved from Maggio et al. (1990). We calculated the X-ray luminosities (L_X) of all stars from the Hipparcos parallaxes. The results are presented in Fig. 8 as a function of $T_{\rm eff}$ for different mass ranges. X-ray luminosities of single giants recently derived from ROSAT data (Pizzolato et al. 2000) are also included. The X-ray emission of giants reaches a maximum value in the effective temperature range 6000 K $< T_{\rm eff} <$ 5000 K corresponding to G spectral types. Figure 8 confirms that the X-ray luminosity of HD 223460 is among the highest within this sample of single nearby F, G and K giants, thus supporting the above evolution scenario. Figure 9 shows that the X-ray-to-bolometric luminosity ratio of HD 223460 is also one of the highest. This indicates that the high X-ray luminosity of HD 223460 results from an increased density of active regions related to its evolutionary position rather than from its large emitting surface. The coronal structure and evolutionary status of HD 223460

would thus be similar to that of FK Comae (Gondoin et al. 2002) and V390 Aurigae (Gondoin 2003). This justifies the classification of HD 223460 as an FK Comae-type star (Fekel & Marshall 1991). These stars seem to be normal 2–3 $M_{\odot}$ giants with A or B type progenitors on the main sequence that are evolving near the bottom of the red giant branch.

7. Summary

The analysis of HD 223460 data suggests that its corona is dominated by the same type of active regions as on the Sun. However, the surface area coverage of these active regions may approach up to 30% and the size of the associated magnetic structures can be similar or larger than that of interconnecting loops between solar active regions while their temperature is hotter. One hypothesis is that the interaction of these structures themselves induces a flaring activity on a small scale not visible in the EPIC light curves that is responsible for heating HD 223460 plasma to coronal temperatures of $T \geq 10^7$ K. The H–R diagram position of HD 223460 suggests that its rotation will spin down in the future with the effect of decreasing its helicity-related, dynamo-driven activity and suppressing large scale magnetic structures in its corona. The coronal structure and evolutionary status of HD 223460 are thus similar to that of FK Comae.

Acknowledgements. I thank my colleagues from the *XMM–Newton* Science Operation Center for their support in implementing the observations. I am grateful to the anonymous referee for the helpful comments that allowed to improve the paper.

References

Anders, E., & Grevesse, N. 1989, Geochim. Cosmochim. Acta, 53, 197
Antonucci, E., & Dodero, M. A. 1995, ApJ, 438, 480
Arnaud, K., & Dorman, B. 2001, XSPEC User's Guide for version 11.1, http://heasarc.gsfc.nasa.gov/docs/xanadu/xspec/manual/manual.html
Audard, M., Güdel, M., & Mewe, R. 2001a, A&A, 365, L318
Audard, M., Behar, E., Güdel, M., et al. 2001b, A&A, 365, L329
Ayres, T. R., Simon, T., Stern, R. A., et al. 1998, ApJ, 496, 428
Bambynek, W., Craseman, B., Fink, R. W., et al. 1972, Rev. Mod. Phys., 44, 716
Bopp, B. W. 1984, ApJS, 54, 387
Bowyer, S., Drake, J. J., & Vennes, S. 2000, ARA&A, 38, 231
Brinkman, A. C., Gunsing, C. J. T., Kaastra, J. S., et al. 2000, ApJ, 530, 111
Brinkman, A. C., Behar, E., Güdel, M., et al. 2001, A&A, 365, L324
Chen, B., Vergely, J. L., Valette, B., & Carraro, G. 1998, A&A, 336, 137
Cowley, A. P., & Bidelman, W. P. 1979, PASP, 91, 83
den Herder, J. W., Brinkman, A. C., Kahn, S. M., et al. 2001, A&A, 365, L7
de Medeiros, J. R., & Lebre, A. 1992, A&A, 264, L21
de Medeiros, J. R., & Mayor, M. 1995, A&A, 302, 745
Dickey, J. M., & Lockman, F. J. 1990, ARA&A, 28, 215
Doschek, G. A., & Cowan, R. D. 1984, ApJS, 56, 67
Drake, J. J., Peres, G., Orlando, S., Laming, J. M., & Maggio, A. 2000, ApJ, 545, 1074
Drake, N. A., Brickhouse, N. S., Kashyap, V., et al. 2001, ApJ, 548, L81
Dupree, A. K., Brickhouse, N. S., Doschek, G. A., Green, J. C., & Raymond, J. C. 1993, ApJ, 418, L41
Durney, B. R., & Latour, J. 1978, Geophysical and Astrophysical Fluid Dynamics, 9, 241
Durney, B. R., De Young, D. S., & Roxburgh, I. W. 1993, Sol. Phys., 145, 207
Ehle, M., Breitfellner, M., Dahlem, M., et al. 2001, The XMM−Newton Users' Handbook, http://xmm.vilspa.esa.es/user/AO2/uhb/xmm_uhb.html
Endal, A. S., & Sofia, S. 1979, ApJ, 232, 531
ESA 1997, The Hipparcos Catalogue, ESA SP-1200
Fekel, F. C., Moffett, T. J., & Henry, G. W. 1986, ApJS, 60
Fekel, F. C., & Marschall, L. A. 1991, AJ, 102, 1439
Feldman P. A. 1982, in Activity in Red Dwarf Stars, ed. M. Rodono, & P. Byrne (Dordrecht: Reidel), IAU Coll., 71, 429
Flower P. J. 1996, ApJ, 469, 335
Gabriel, A. H., & Jordan, C. 1969, MNRAS, 145, 241
Gilliland, R. L. 1985, ApJ, 299, 286
Golub, L., & Pasachoff, J. M. 1997, in The Solar Corona (Cambridge, UK: Cambridge University Press)
Gondoin, P. 1999, A&A, 352, 217
Gondoin, P., Aschenbach, B., Erd, C., et al. 2000, SPIE Proc., 4140, 1
Gondoin, P., Erd, C., & Lumb., D. 2002, A&A, 383, 919
Gondoin, P. 2003, A&A, 404, 355
Gray, D. F. 1989, ApJ, 347, 1021
Gray, D. F., & Endal, A. S. 1982, ApJ, 254, 162
Griffiths, N. W., & Jordan, C. 1998, ApJ, 497, 1998
Güdel, M. 1997, ApJ, 480, L121
Güdel, M., Guinan, E. F., Mewe, R., Kaastra, J. S., & Skinner, S. L. 1997a, ApJ, 479, 416
Güdel, M., Guinan, E. F., & Skinner, S. L. 1997b, ApJ, 483, 947
Güdel, M., Audard, M., Magee, H., et al. 2001, A&A, 365, L344
House, L. L. 1969, ApJS, 18, 2
Huenemoerder, D. P., Canizares, C. R., & Schulz, N. S. 2001, ApJ, 559, 1135
Hünsch, M., Schmitt, J. H. M. M., & Voges, W. 1998, A&AS, 127, 251
Jansen, F., Lumb, D., Altieri, B., et al. 2001, A&A, 365, L1
Johnson, O., Drake, J. J., Kashyap, V., et al. 2002, ApJ, 565, L97
Kurucz, R. L. 1991, in Stellar Atmospheres: Beyond Classical Models, NATO ASI Series C, vol. 341
Liedahl, D. A., Osterheld, A. L., & Goldstein, W. H. 1995, ApJ, 438, 115
Maggio, A., Vaiana, G. S., Haisch, B. M., et al. 1990, ApJ, 348, 253
Makishima, K. 1986, in The Physics of Accretion onto Compact Objects, p. 250, ed. K. O. Mason, M. G. Watson, & N. E. White (Springer Verlag: Berlin)
Mewe, R., Gronenschild, E. H. B. M., Heise, J., et al. 1982, ApJ, 260, 233
Mewe, R., Gronenschild, E. H. B., & van den Oord, G. H. J. 1985, A&A, 62, 197
Mewe, R., Kaastra, J. S., White, S. M., & Pallavicini, R. 1996, A&A, 315, 170
Mewe, R., Raassen, A. J. J., Drake, J. J., et al. 2001, A&A, 368, 888
Murphy, R. J., Ramaty, R., Reames, D. V., & Koslovsky, B. 1991, ApJ, 371, 793
Parker, E. N. 1955, ApJ, 122, 293
Pizzolato, N., Maggio, A., & Sciortino, S. 2000, A&A, 361, 614
Pradhan, A. K. 1982, ApJ, 263, 477
Raymond, J. C., & Smith, B. W. 1977, ApJS, 35, 419
Reale, F., Peres, G., & Orlando, S. 2001, ApJ, 557, 906

Rogers F. J., & Iglesias, C. A. 1992, ApJS, 79, 507
Rosner, R., Tucker, W. H., & Vaiana, G. S. 1978, ApJ, 220, 643
Rosner, R., Musielak, Z. E., Cattaneo, F., Moore, R. L., & Suess, S. T. 1995, ApJ, 442, L25
Rutten, R. G. M., & Pylyser, E. 1988, A&A, 191, 227
SAS 2001, XMM-Newton Science Analysis System, Reference Documentation, http://xmm.vilspa.esa.es/user/sas_top.html
Sanz-Forcada, J., Brickhouse, N. S., & Dupree, A. K. 2002, ApJ, 570, 799
Schaller, G., Schaerer, D., Meynet, G., & Maeder, A. 1992, A&AS, 96, 269
Schmelz, J. T. 1993 ApJ, 408, 373
Schmitt, J. H. M. M., Drake, J. J., & Stern, R. A. 1996, ApJ, L465, 51
Schrijver, C. J., Mewe, R., van den Oord, G. H. J., & Kaastra, J. S. 1995, A&A, 302, 438
Simon, T., & Drake, S. A. 1989, ApJ, 346, 303
Singh, K. P., Drake, S. A., White, N. E., & Simon, T. 1996, AJ, 112, 221
Strassmeier, K. G., & Hall, D. S. 1988, ApJS, 67 453
Strüder, L., Briel, U., Dennerl, K., et al. 2001, A&A, 365, L18
Tsuru, T., Makishima, K., Ohashi, T., et al. 1989, PASJ, 41, 679
Turner, M. J. L. T., Abbey, A., Arnaud, M., et al. 2001, A&A, 365, L27
Vaiana, G. S., Davis, J. M., Giacconi, R., et al. 1973, ApJ, 185, 47
Vaiana, G. S., & Rosner, R. 1978, ARA&A, 16, 393
van den Oordt, G. H. J., & Mewe, R. 1989, A&A, 213, 245
Van Speybroeck, L. P., Krieger, A. S., & Vaiana, G. S. 1970, Nature, 227, 818
Wallerstein, G., Bohm-Vitense, E., Vanture, A. D., & Gonzales, G. 1994, AJ, 107, 2211